

Ensemble forecasting of coronal mass ejections using the WSA-ENLIL with Coned Model

D. Emmons,¹ A. Acebal,¹ A. Pulkkinen,² A. Taktakishvili² and P. MacNeice²

Abstract. The combination of the Wang-Sheeley-Argé (WSA) coronal model, ENLIL heliospherical model version 2.7, and Coned Model version 1.3 (WSA-ENLIL with Coned Model) was employed to form ensemble forecasts for 15 halo-coronal mass ejections (CMEs). The input parameter distributions were formed from 100 sets of CME cone parameters derived from the Coned Model. The Coned Model used image processing along with the bootstrap approach to automatically calculate cone parameter distributions from SOHO/LASCO imagery based on techniques described by *Pulkkinen et al.* [2010]. The input parameter distributions were used as input to WSA-ENLIL to calculate the temporal evolution of the CMEs, which were analyzed to determine the propagation times to the L₁ Lagrangian point and the maximum K_p indices due to the impact of the CMEs on the Earth's magnetosphere. The *Newell et al.* [2007] maximum K_p index formula was employed to calculate the maximum K_p indices based on the predicted solar wind parameters near Earth using two magnetic field orientations: completely southward magnetic field and expected value for the clock-angle term in the *Newell et al.* [2007] maximum K_p index formula. The forecasts for 5 of the 15 events had accuracy such that the actual propagation time was within the ensemble average plus or minus one standard deviation, and 8 of the 15 events had the actual propagation time within the range of the ensemble. For the completely southward magnetic field assumption, 10 of the 15 events were forecast with accuracy such that the actual maximum K_p index was within the range of the ensemble, and the forecasts for 9 of the 15 events contained the actual maximum K_p index when using the expected value for the clock-angle term. The mean absolute forecast errors were calculated to be 9.1 *hours* for the propagation time, 1.7 for the maximum K_p index using the completely southward magnetic field, and 1.8 using the expected value of the clock-angle term.

1. Introduction

Coronal mass ejections (CMEs) are the cause of the most severe geomagnetic storms [*Gosling, 1993*]. Geomagnetic storms can cause a variety of problems at Earth including radio wave propagation disruption [*Tascione, 1994*], degradation of satellite performance [*Afraimovich et al., 2003*], and disruption of electrical systems on the Earth's surface [*Boteler et al., 1998*]. For these reasons, the scientific community has a great interest in predicting the arrival times and impacts of CMEs at Earth.

A number of models have been developed to estimate the propagation time of CMEs. Some of the earlier models were shock propagation models based on type II meter wave burst measurements, such as the Shock Time of Arrival (STOA) model [*Dryer, 1974*] and the Interplanetary Shock Propagation Model (ISPM) [*Smith and Dryer, 1990*]. Empirical forecast models have been developed recently, including the model developed by *Gopalswamy et al.* [2001] which treats the CME as a kinematic object which experiences accelerations or decelerations to match the ambient solar wind speed at distances near 1 *AU*.

The most current and advanced method of forecasting CMEs is based on numerically solving the magnetohydrodynamic (MHD) equations governing the motion of the CME

over time. ENLIL is a time-dependent three-dimensional model which solves the MHD equations for plasma mass, momentum, magnetic field, and energy density using a finite difference approximation [*Odstrčil and Pizzo, 1999*]. ENLIL can accept the output of the Wang-Sheeley-Argé (WSA) coronal model for use as the inner boundary condition in the finite difference computations, which calculates the background solar wind solution and interplanetary magnetic field (IMF) polarity based on solar magnetogram measurements [*Argé and Pizzo, 2000*]. ENLIL can also accept the output of the Cone Model to initialize the CME velocity, angular width, and axis of propagation.

The Cone Model, developed by *Zhao et al.* [2002], assumes that the CME has the shape of a cone with constant angular width, propagates in a radial direction, and experiences isotropic expansion. A technique to manually determine the cone parameters from SOHO/LASCO imagery was developed by *Xie et al.* [2004]. Previous analyses have been completed using the analytic Cone Model along with WSA-ENLIL to forecast the propagation times and impacts of CMEs, and have showcased the effectiveness of the WSA-ENLIL with Cone Model combination (e.g. *Taktakishvili et al.* [2009], *Taktakishvili et al.* [2010]).

The analytic Cone Model relies on a manual determination of the CME outer boundary from LASCO imagery. The development of the Coned Model, an automated version of the Cone Model, removed the user from the process of manually determining the CME outer boundary [*Pulkkinen et al., 2010*]. The Coned Model uses image processing to automatically determine the location of the CME mass from a time-series of LASCO images, and then calculates a distribution of possible cone parameters using the bootstrap approach. The distribution of cone parameters allows

¹Department of Engineering Physics, Air Force Institute of Technology, Dayton, Ohio, USA.

²NASA Goddard Space Flight Center, Greenbelt, Maryland, USA.

for a dynamic quantification of the uncertainty of the cone parameters based on LASCO imagery, which will vary for each event.

The performance of the WSA-ENLIL with Coned Model has been analyzed with the median values of the cone parameter distributions used as input for a single WSA-ENLIL run. The *Taktakishvili et al.* [2011] analysis showed that the analytic Cone Model and the Coned Model (automatic Cone Model) had reasonable agreement in the forecasts with a mean absolute propagation time forecast error of 6.9 *hours* for the analytic Cone Model and 11.2 *hours* for the Coned Model. The performance of the WSA-ENLIL with Coned Model version 1.2 was analyzed by *Falkenberg et al.* [2011], with the conclusion that the CME velocity and angular width were underestimated by the Coned Model. Coned Model version 1.3 is the most current version of the Coned Model, and has included a modification in the optimization routine to increase the CME velocity and width estimations following the results of the *Falkenberg et al.* [2011] analysis.

With the production of the cone parameter distributions from the Coned Model readily available, an ensemble forecast can be calculated. The weather community has long known of the improvement in forecast accuracy due to the use of ensemble forecasting [*Leith, 1974*]. Ensemble forecasting also allows for a quantification of forecast uncertainty based on uncertainty in the measurements of the initial conditions, which is impossible for single forecasts. This quantification of forecast uncertainty could provide useful information to operational forecasts of CMEs.

This analysis applied the ensemble forecasting technique to 15 halo-CMEs using the WSA-ENLIL with Coned Model. The ensembles were created from 100 sets of initial states (cone parameters), derived from Coned Model version 1.3, which were used as input to WSA-ENLIL version 2.7 to obtain distributions of future states. The distributions of future states were analyzed to produce distributions of propagation time forecasts to the L_1 Lagrangian point and distributions of maximum K_p index forecasts due to the impact of the CME on the Earth's magnetosphere.

2. Brief Description of WSA, ENLIL, and Coned Model

In 2009, *Pulkkinen et al.* created the Coned Model, which determines the cone parameters from a time-series of LASCO C3 images automatically. The cone parameters are composed of the radial velocity of the cone-front, the angular width of the cone, and the propagation axis (direction of propagation) of the cone. The Coned Model uses image processing to automatically determine the location of the CME mass from LASCO imagery by filtering the image based on a brightness threshold, which differentiates the brighter CME mass location from the darker image background. The bootstrap approach is used to determine the confidence intervals for the calculated cone parameters by randomly selecting 300 points from the CME mass locations in the filtered LASCO images, then calculating the best-fitting cone to the randomly selected points. The process can be repeated any number of times, to create a distribution of cone parameters for the CME of interest.

The Wang-Sheely-Arge (WSA) model is an empirical model used to calculate background solar wind speed and interplanetary magnetic field polarity [*Arge and Pizzo, 2000*]. The model calculates the magnetic field between the solar surface, based on synoptic magnetogram data, and a boundary sphere where the magnetic field is assumed to be radial. The solar wind speed at the boundary sphere is calculated using an inverse relationship between the solar wind speed and the magnetic expansion factor. WSA creates the inner

boundary conditions for ENLIL, which controls the ambient solar wind conditions and IMF structure in the ENLIL computations.

After the input parameters are obtained from the Coned Model and the boundary conditions are obtained from the WSA model, ENLIL approximates the time dependent solution to the MHD equations governing the plasma from 21.5 solar radii to an appropriate outer boundary (1.1 AU for analyzing the effects of a CME near Earth). ENLIL utilizes a modified Total-Variational-Diminishing Lax-Friedrich (TVDLF) finite difference scheme to approximate the solution to the partial differential MHD equations [*Tóth and Odstrčil, 1996*]. The current version of ENLIL assumes no internal magnetic field structure to the CME, but allows the propagation of the CME to distort the interplanetary magnetic field structure.

3. Ensemble Forecasting

Formally, ensemble forecasting can be described by a transition from a probability distribution of initial states, $p(\bar{v}_t|\bar{o}_t)$, given a set of observations, \bar{o}_t , to a probability distribution of future states, $p(\bar{v}_{t+\tau}|\bar{o}_t)$:

$$p(\bar{v}_{t+\tau}|\bar{o}_t) = \int r(\bar{v}_{t+\tau}|\bar{v}_t)p(\bar{v}_t|\bar{o}_t)d\bar{v}_t, \quad (1)$$

where \bar{v}_t is the initial state, $\bar{v}_{t+\tau}$ is the future state, $r(\bar{v}_{t+\tau}|\bar{v}_t)$ is the transition probability associated with the forecasting model, and the integral is a multiple integral [*DelSole, 2005*]. For a deterministic model (a model which provides the same result if run multiple times with the same set of initial conditions), such as ENLIL, the transition probability can be described by a delta function.

The ensemble forecast distribution for a particular set of observations can be calculated from the probability distribution of future states, which provides more information than a traditional single forecast. The ensemble forecast distribution can be statistically analyzed to obtain the mean or median value of a particular parameter of interest, along with the associated uncertainty of the value. The range of

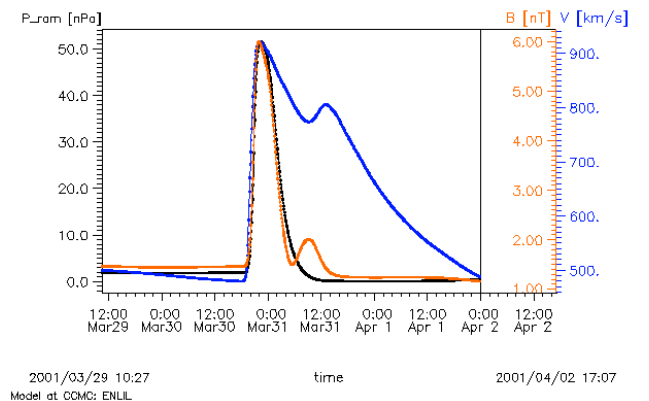


Figure 1. The solar wind dynamic pressure, velocity and magnetic field magnitude at Earth calculated using WSA-ENLIL for the 29 Mar 2001 CME. The large increase in dynamic pressure is associated with a large increase in the first temporal derivative, and is indicative of the CME arrival at Earth. This plot was created using the Community Coordinated Modeling Center's (CCMC's) on-line visualization tools (<http://ccmc.gsfc.nasa.gov/>).

the ensemble forecast distribution provides the range of possible outcomes for a given set of observations.

For this analysis, an ensemble forecast was calculated for a total of 15 halo-CMEs using the WSA-ENLIL version 2.7 with Coned Model version 1.3. For each CME, the Coned Model was used to sample 100 sets of initial conditions from the probability distribution of initial states based on three LASCO C3 images of the CME eruption with a temporal spread of at least one hour between the first and the last image. The 100 sets of initial conditions were then used as input WSA-ENLIL to obtain the probability distributions of future states, which were used to calculate the ensemble forecast distributions. The ensemble forecasting process used for this analysis can be summarized by

$$\begin{aligned} \text{LASCO C3 Images} &\rightarrow \bar{o}_t \rightarrow \text{Coned Model} \rightarrow & (2) \\ p(\bar{v}_t|\bar{o}_t) &\rightarrow \text{WSA-ENLIL} \rightarrow p(\bar{v}_{t+\tau}|\bar{o}_t). \end{aligned}$$

Two parameters were calculated from $p(\bar{v}_{t+\tau}|\bar{o}_t)$ to obtain the ensemble forecast distributions: the propagation time of the CME to the L_1 Lagrangian point, and the maximum K_p index due to the CME impact on the Earth's magnetosphere. For this analysis, the resolution of the computational grid used by ENLIL ($r \times \theta \times \phi = 160 \times 30 \times 90$) placed the L_1 Lagrangian point and Earth in the same sector, so the computed propagation time to Earth was the same as the computed propagation time to the L_1 Lagrangian point.

The arrival time of the CME at Earth was selected to be the time at which the first temporal derivative of the solar wind dynamic pressure at Earth, calculated from ENLIL output, experienced a large increase in magnitude (Figure 1). The arrival time could also be considered to be the time at which the second temporal derivative of the dynamic pressure was a maximum. To ensure that the arrival times calculated by the first derivative were not falsely triggered, the arrival times calculated by the first derivative were compared to the arrival times calculated by the maximum second derivative, and they were found to be in good agreement (results not shown).

The maximum K_p indices were found using the *Newell et al.* [2007] maximum K_p formula:

$$\begin{aligned} K_p &= 0.0002947 \left(\frac{d\Phi_{MP}}{dt} \right) + 1 & (3) \\ &= 0.0002947 \left(v^{4/3} B_T^{2/3} \sin^{8/3} [\theta_c/2] \right) + 1, \end{aligned}$$

where $d\Phi_{MP}/dt$ is the solar wind-magnetosphere coupling function, v is the speed (km/s) at which the interplanetary magnetic field (IMF) lines approach the magnetopause and can be approximated by the solar wind speed, B_T is the magnitude of the IMF (nT), and θ_c is the IMF clock angle defined by $\theta_c = \arctan(B_y/B_z)$. The magnetic field orientation of the CME "cloud" was not available from ENLIL, so two magnetic field orientations were assumed and analyzed: First, the magnetic field was assumed to be completely southward ($\theta_c = \pi$), in order to calculate the worst-case scenario. Second, the expected value of the clock-angle term in the *Newell et al.* [2007] formula was used, assuming the magnetic field clock-angle was randomly oriented with a uniform distribution. For a randomly oriented clock angle with a uniform distribution, the expected value of the clock-angle term was calculated to be

$$\left\langle \sin^{8/3} \left(\frac{\theta_c}{2} \right) \right\rangle = \frac{1}{2\pi} \int_0^{2\pi} \sin^{8/3} \left(\frac{\theta_c}{2} \right) d\theta_c \approx 0.45. \quad (4)$$

The K_p indices were rounded to the nearest integer value. Also, the K_p index has a maximum value of nine, so any calculations of the maximum K_p index using the *Newell et al.* [2007] formula exceeding nine were limited to nine.

Eight of the CMEs studied in this analysis were selected from the *Taktakishvili et al.* [2011] analysis, based on CMEs

which caused particularly large geomagnetic storms. The other seven CMEs were selected based on the fact that they had a maximum K_p of less than eight, and that there were no other halo-CMEs within plus or minus two days from the eruption day of the CME. The selected CMEs were required to have clear LASCO C3 images to run the Coned Model, and clear ACE data to determine the actual arrival times of the CMEs at the L_1 Lagrangian point. The CMEs were also selected with a large variety of associated solar flare locations in order to analyze the performance of the model with CMEs initiated from a variety of locations.

The calculated propagation times were compared to the actual propagation times derived from ACE measurements, with 10 *minute* resolution. The actual arrival times calculated directly from ACE data were compared to the arrival times logged in the National Oceanic and Atmospheric Administration (NOAA) Space Weather Prediction Center's (SWPC) historical weekly reports (<http://www.swpc.noaa.gov/ftpmenu/warehouse.html>) to ensure consistency.

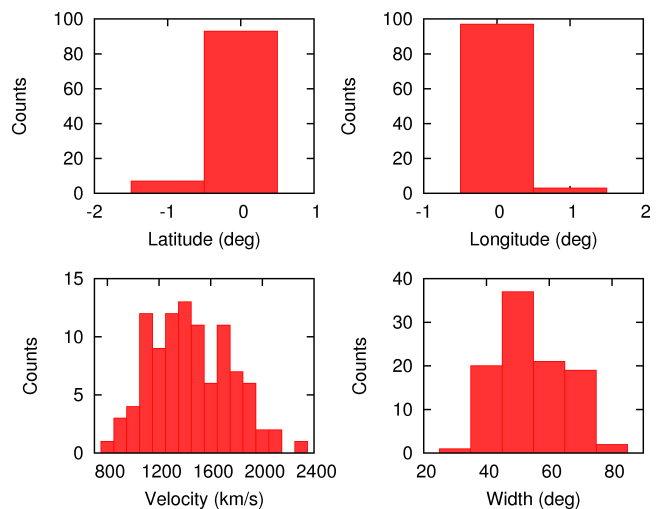


Figure 2. The cone parameter distributions, derived from the Coned Model, for the 29 Mar 2001 CME (event 4). The count number is the number of times a cone parameter was within the range of a bin, for the 100 sets of cone parameters.

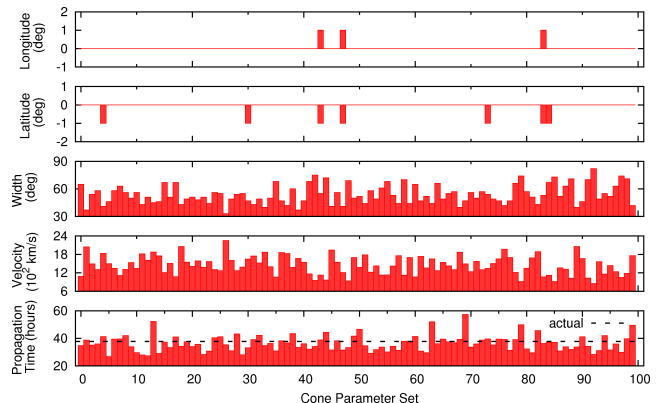


Figure 3. The cone parameters and propagation time forecasts for each of the 100 sets of parameters composing the ensemble for the 29 Mar 2001 CME (event 4). Each set of cone parameters maps to a propagation time, which shows the relationship between the cone parameters and the ensemble forecast.

Table 1. The start date and times, actual propagation times as measured by ACE, actual maximum K_p indices, and the locations of the associated solar flares for the 15 CMEs analyzed. The CMEs were also labeled with an event number for quick reference.

event number	CME start date (YYYYMMDD)	CME start time (UT)	propagation		associated solar flare location
			time to ACE (HH:MM)	maximum K_p	
1	19990503	06:06	56:50	3	N15E32
2	20000404	16:32	47:30	9	N16W66
3	20000714	10:54	27:20	9	N22W07
4	20010329	10:26	37:50	9	N20W19
5	20010410	5:30	33:50	8	S23W09
6	20010924	10:30	33:30	7	S16E23
7	20011009	11:30	52:45	6	S28E08
8	20011104	16:35	32:40	9	N06W18
9	20011117	05:30	60:00	4	S13E42
10	20031028	11:30	18:20	9	S16E08
11	20031029	20:54	19:50	9	S15W02
12	20040720	13:31	44:20	7	N10E35
13	20041106	02:06	39:40	9	N07E00
14	20041203	00:26	54:20	4	N09E03
15	20100403	10:34	45:15	8	S25E00

The calculated maximum K_p indices were compared to the actual ground-based maximum K_p values, with integer resolution. The actual maximum K_p indices were found using NASA’s OMNIWeb database (<http://omniweb.gsfc.nasa.gov/form/dx1.html>). The solar flare locations were derived from the NOAA/SWPC historical solar events reports, which provided the approximate locations of the CME eruptions. The measured values for the actual propagation times, maximum K_p indices, and locations of the associated solar flares are displayed in Table 1.

4. Results: Single Event

The ensemble distributions for the 29 Mar 2001 CME (event 4) are displayed in this section as an example of the results obtained for each of the events analyzed. For the

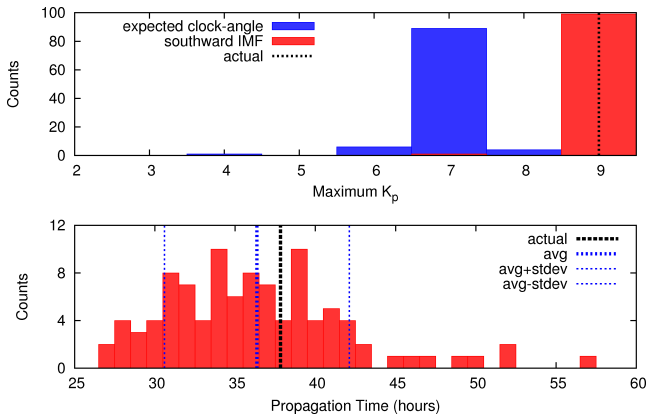


Figure 4. The maximum K_p index and propagation time distributions, for the 29 Mar 2001 CME (event 4). The count number is the number of times a cone parameter was within the range of a bin, for the 100 sets of results derived from the 100 sets of cone parameters. The “southward IMF” describes the maximum K_p index calculations using a completely southward magnetic field, and the “expected clock-angle” describes the calculations using the expected value for the clock angle term in the *Newell et al.* [2007] formula.

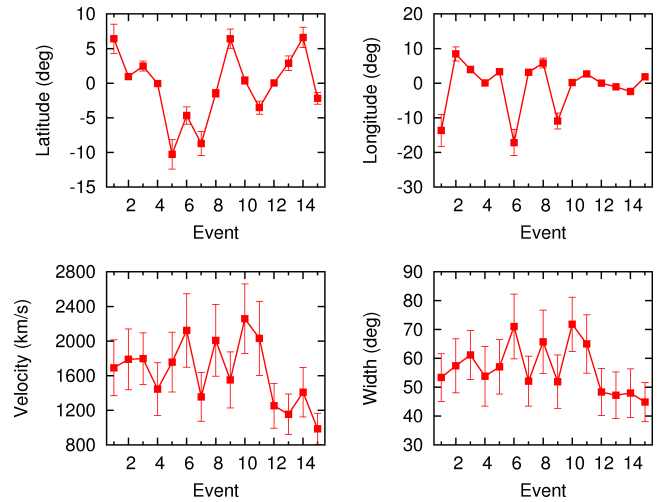


Figure 5. The averages and standard deviations of the cone parameter distributions, derived from Coned Model version 1.3, for each event. The Coned Model used three LASCO C3 images of the CME eruption to develop the distributions of cone parameters, for each CME.

29 Mar 2001 CME, the ensemble produced by the Coned Model had an average velocity of 1444.3 km/s with a standard deviation of 304.9 km/s (Figure 2). The angular width ensemble had an average of 53.8° with a standard deviation of 10.3° . The propagation axis latitude ensemble had an average of -0.1° with a standard deviation of 0.3° . The propagation axis longitude ensemble had an average of 0.0° with a standard deviation of 0.2° .

Each of the 100 sets of cone parameters mapped to a separate forecast (Figure 3). The set of 100 forecasts created by the 100 sets of cone parameters formed the ensemble forecast (Figure 4). The ensemble forecast was analyzed to obtain a single forecast along with the uncertainty in the forecast (width of the ensemble). The average of the propagation time ensemble was used as the single forecast for the propagation time, and the median of the maximum K_p index ensemble was used as the single forecast for the maximum K_p index (the rounded average was the same as the median

for all events). The standard deviations and ranges were used to describe the width of the ensembles.

For the 29 Mar 2001 CME, the average of the propagation time ensemble was 36.4 hours with a standard deviation of 5.8 hours. With an actual propagation time of 37.8 hours, the absolute forecast error was 1.5 hours. Using the completely southward magnetic field assumption, the median of

the maximum K_p ensemble was calculated to be 9, with a range of 2 (the standard deviation was 0.2, which was too small to represent the uncertainty for the integer resolution used for the K_p). Using the expected value for the clock-angle term in the *Newell et al.* [2007] maximum K_p formula, the ensemble median was 7, with a range of 4. The actual maximum K_p index was 9, which indicated that the completely southward magnetic field predicted the magnitude perfectly, while using the expected value for the clock-angle term underestimated the magnitude by 2.

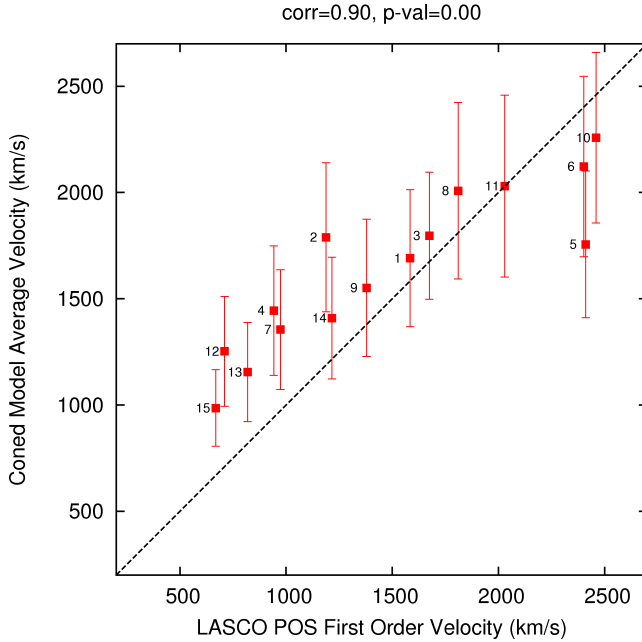


Figure 6. The Coned Model average velocities versus the LASCO first-order POS velocities, with the event number as the label and the standard deviations of the ensembles as the error bars. The two methods of calculating the CME velocities were strongly correlated, with the Coned Model velocities 156.2 km/s faster than the LASCO first-order POS velocities, on average.

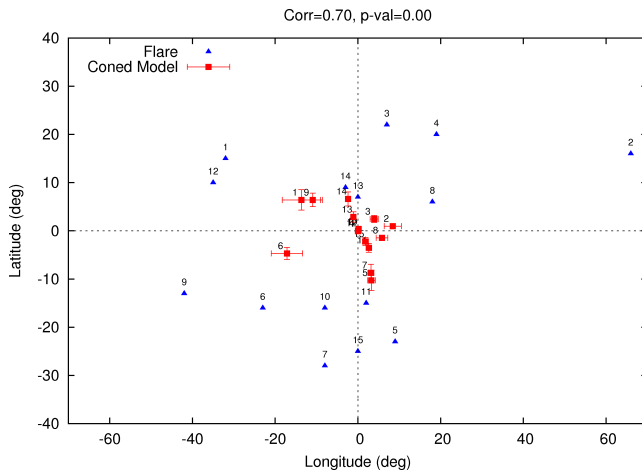


Figure 7. The Coned Model average longitudes and latitudes along with the associated solar flare latitudes and longitudes, with the event numbers as the labels and the standard deviations of the ensembles as the error bars. Relative to the associated solar flare locations, the Coned Model propagation axes tended to be pushed towards the Sun-Earth line.

5. Results: Cone Parameters

The cone parameter distribution widths, for the 15 CMEs, were averaged to obtain a measure of the cone parameter uncertainty derived from LASCO imagery via the Coned Model. The average of the standard deviations were 323.6 km/s for the velocity ensembles, 9.1° for the angular width ensembles, 1.0° for the latitude ensembles, and 1.3° for the longitude ensembles (Figure 5). The average of the ranges were 1615.0 km/s for the velocity ensembles, 45.0° for the angular width ensembles, 4.0° for the latitude ensembles, and 4.0° for the longitude ensembles. This indicated that the width of the propagation axis ensembles tended to be more narrow than the velocity and angular width ensembles.

The averages of the Coned Model velocity distributions displayed a strong positive correlation with the LASCO first-order plane of sky (POS) velocities (Figure 6). The LASCO first-order POS velocities were the first-order (linear) fits to the leading edge of the CMEs in the POS from LASCO imagery (http://cdaw.gsfc.nasa.gov/CME_list/), and provided an estimate of the two-dimensional POS velocity of the CMEs. The average difference between the Coned Model average velocities and the LASCO first-order POS velocities was 156.2 km/s, which indicated that the Coned Model velocities tended to be faster than the LASCO first-order POS velocities. This was consistent with the fact that the

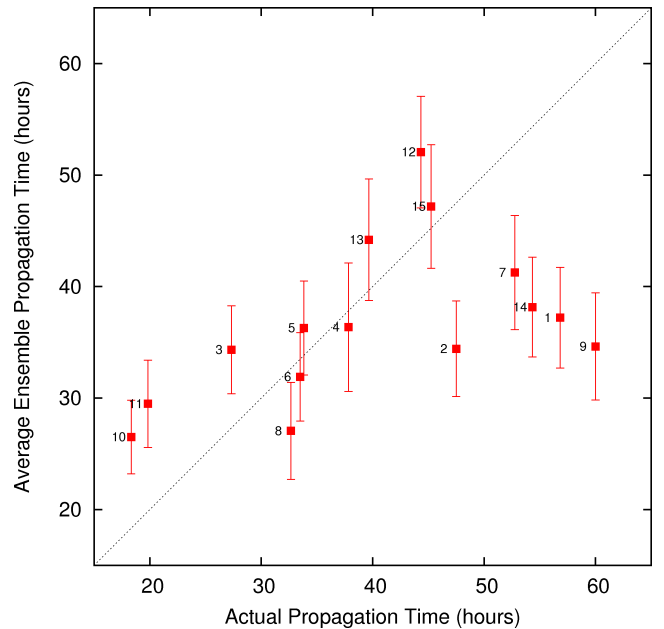


Figure 8. The averages and standard deviations of the propagation time ensembles versus the actual propagation times, with the event number as the label. The actual propagation time was within the average plus or minus one standard deviation for 5 of the 15 events.

Coned Model predicted the radial (three-dimensional) velocity, while the LASCO first-order POS velocity was a measure of the two-dimensional POS velocity.

Relative to the locations of the associated solar flares, the Coned Model tended to push the propagation axis of the CMEs towards the Sun-Earth line (Figure 7). The Coned Model calculated propagation axes with average latitude or longitude magnitudes greater than 10° for only 4 of the 15 CMEs. While the location of the associated solar flare is not necessarily an indicator of the direction of the CME prop-

agation, 13 of the 15 associated solar flare locations were located elsewhere on the disk than between $\pm 10^\circ$ for either latitude or longitude.

6. Results: Propagation Time

The ensemble forecasts predicted 5 of the 15 propagation times with accuracy such that the actual propagation time was within the average plus or minus one standard deviation (Figure 8). All 5 of these CMEs had actual propagation times between 30 and 46 hours. Only 2 of the 7 CMEs with actual propagation times between 30 and 46 hours were not accurate enough to predict the actual propagation time within the average plus or minus one standard deviation.

The actual propagation time for 8 of the 15 ensemble forecasts were within of the range of the ensemble distribution (Figure 9). Of the 8 forecasts, 7 were for CMEs with actual

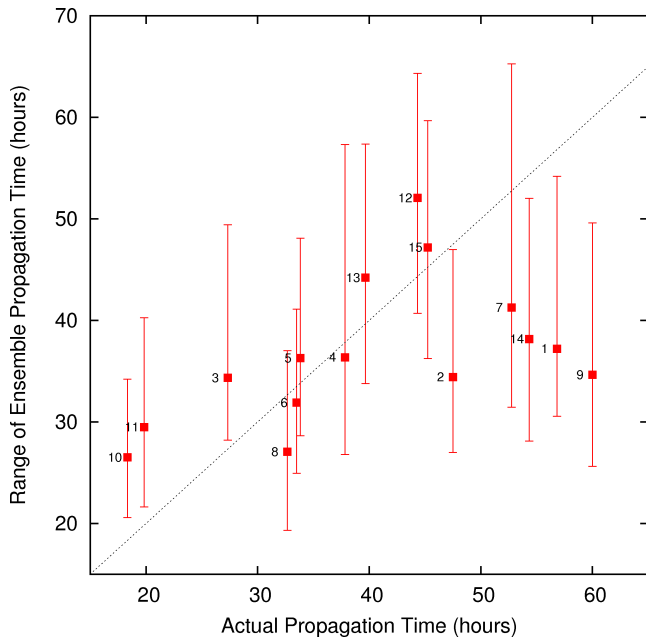


Figure 9. The averages and ranges of the ensemble propagation times versus the actual propagation times, with the event number as the label. The actual propagation time was within the ensemble range for 8 of the 15 events.

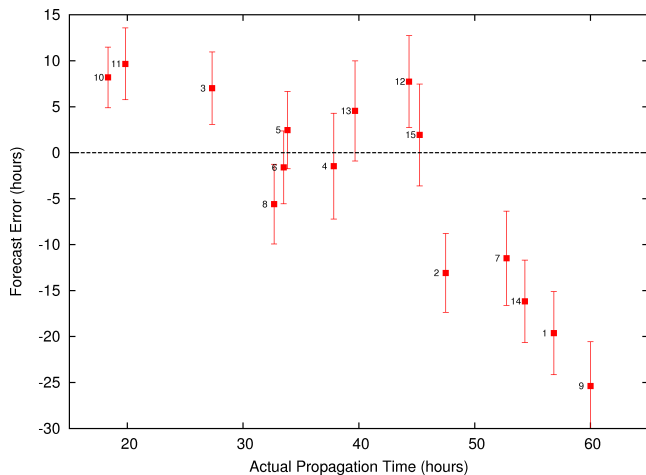


Figure 10. The propagation time forecast error versus the actual propagation time, with the error bars as one standard deviation and the labels as the event number. The forecasts for the events with actual propagation times between 27 and 46 hours were the most accurate, while the largest forecast errors were for the events with actual propagation times greater than 46 hours.

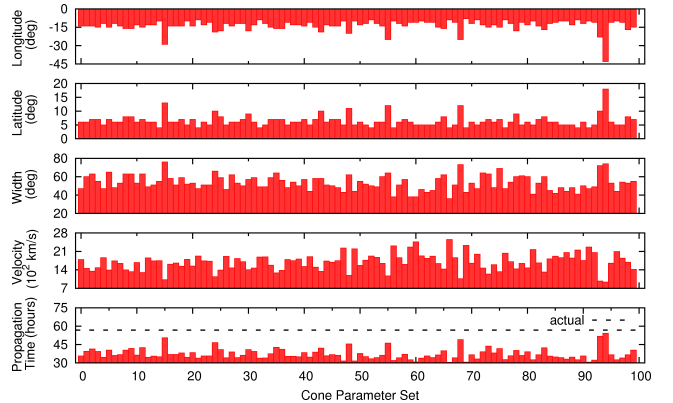


Figure 11. The cone parameters and propagation time forecasts for each of the 100 sets of parameters composing the ensemble for event 1 (3 May 1999 CME). The inverse relationship between the magnitude of the propagation axis angles (latitude/longitude) and the velocity is apparent.

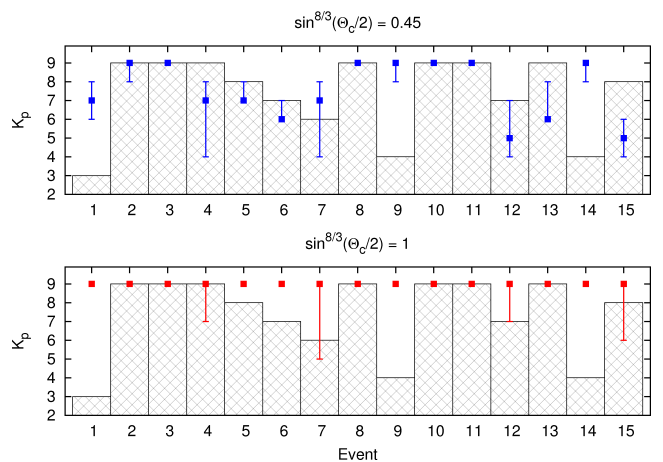


Figure 12. The median and range of the maximum K_p , per event, using both the expected value for the clock-angle term in the *Newell et al.* [2007] formula (top) and assuming the magnetic field is completely southward (bottom). The points with error bars are from the ensemble forecasts, and the bars are the actual maximum K_p indices.

propagation times between 30 and 46 hours, and the remaining forecast was for a CME with an actual propagation time around 53 hours. All 7 of the CMEs analyzed with actual propagation times between 30 and 46 hours were accurate enough to predict the actual propagation time inside of the range of the ensemble.

The average of the ensemble standard deviations was calculated to be 4.6 *hours*, with a standard deviation of 0.7 *hours*. This quantification of the propagation time uncertainty was based strictly on the uncertainty in the initial conditions calculated from LASCO imagery of the CMEs of interest. Another measure of the propagation time uncertainty was the range of the ensembles, which were averaged to obtain 22.2 *hours*, with a standard deviation of 5.2 *hours*. While this was too large of an uncertainty to be useful for operational forecasts, it was an important metric to analyze the overall performance of the ensemble forecasting technique. The quantification of the uncertainty provided an estimate of the widths of the ensembles, and was not a measure of the forecast error.

The forecast error for the propagation time was defined as the ensemble average minus the actual propagation time. The ensemble forecasts for the 8 events with actual propagation times between 27 *hours* and 46 *hours* were the most accurate of the 15 forecasts, with all of the absolute forecast errors less than 8 *hours* (Figure 10). The forecast errors for the two fast CMEs, events 10 and 11 (28 and 29 Oct 2003 CMEs), were around 9 *hours* indicating that the CME velocities were underestimated. The absolute forecast errors for events with actual propagation times less than 46 *hours* were less than 10 *hours*, while the absolute forecast errors for events with actual propagation times greater than 46 *hours* were all greater than 10 *hours*.

The forecast error for the slow CMEs, with actual propagation times over 46 *hours*, were all less than -10 *hours*. This indicated that the ensemble forecasts greatly underestimated the propagation times of the slower CMEs. For the events with actual propagation times greater than 50 *hours*, the absolute forecast error increased as the actual propagation time increased. The slowest event (event 9), had an actual propagation time of 60.0 *hours* and a forecast error of -25 *hours*.

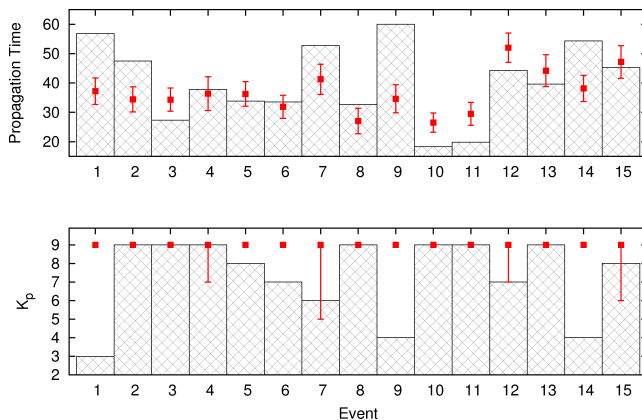


Figure 13. The median and range of the maximum K_p index ensemble using the completely southward magnetic field assumption, along with the average and standard deviation of the propagation time, per event, for the 15 CMEs. The ensemble forecasts and uncertainties are the points with the error bars, and the bars are the actual values. The events with the largest propagation time errors also had the largest maximum K_p errors, which was due to overestimations of the CME velocities.

The large forecasting errors for the slower CMEs were most likely due to the combination of velocity overestimations and misrepresentations of the propagation axis orientations. The Coned Model tended to push the propagation axes towards the Sun-Earth line, which may not have been an accurate representation for all of the actual propagation axes (STEREO data was only available for event 15, so it could not be used to determine the actual propagation axes). The optimization routine used by the Coned Model to calculate the cone parameters forced the CME velocity to have an inverse relationship to the magnitude of the propagation axis angles (latitude/longitude) and the angular width. This relationship is apparent from Figure 11, where cone parameters and propagation times for each of the 100 sets of parameters composing the ensemble are displayed separately, for event 1 (3 May 1999 CME). The sets of cone parameters with the largest magnitudes for the propagation axis angles also had the slowest velocities, and therefore the greatest propagation times. For the slower events, the selection of propagation axis angles close to the Sun-Earth line forced the selection of faster velocities, which resulted in underestimated propagation times.

The mean absolute forecast error, for the 15 CMEs, was calculated to be 9.1 *hours* with a standard deviation of 7.1 *hours*. This mean absolute forecast error was greater than the mean absolute error of 6.9 *hours* found by *Taktakishvili et al.* [2011] using single ENLIL runs with the analytical Cone Model, but was less than the 11.2 *hour* mean absolute error found by *Taktakishvili et al.* [2011] using single ENLIL runs with the median values of the cone parameters derived from the Coned Model. It must be noted that the *Taktakishvili et al.* [2011] analysis did not use the same set of events as this analysis, so the results are not directly comparable.

7. Results: Maximum K_p Index

7.1. Completely Southward Magnetic Field

The ensemble forecast tended to overestimate the magnitude of the impacts of the CMEs by forecasting a maximum K_p of 9 for all 15 CMEs using the completely southward magnetic field assumption (Figure 12). Of the 15 CMEs, 7 had an actual maximum K_p of 9, and 3 had an actual maximum K_p less than 5. Therefore, 7 of the CME impacts were forecast perfectly, and 3 were greatly overestimated. The ensemble forecasts for 10 of the 15 CMEs had accuracy such that the actual maximum K_p was within the range of the ensemble. Of the 8 events with actual maximum K_p indices less than 9, 3 forecasts contained the actual maximum K_p inside of the range of the ensemble.

The average of the ensemble ranges was calculated to be 0.7 with a standard deviation of 1.3. The ensemble ranges were zero for all but 4 events, which was due to the overestimation of the maximum K_p values and the fact that any maximum K_p calculation exceeding 9 was limited to 9. For the events with non-zero uncertainties, the average of the ensemble ranges was calculated to be 2.8. This provided a quantification of the uncertainty in the maximum K_p calculations, and was not a measure of the forecast error.

The forecast error for the maximum K_p was defined as the ensemble median minus the actual maximum K_p . The mean absolute forecast error, for all 15 events, was calculated to be 1.7 with a standard deviation of 2.1. The mean absolute forecast error for the 7 events with actual maximum K_p indices equal to 9 was 0.0, and the mean absolute forecast error for the 8 events with actual maximum K_p indices less than 9 was 3.1.

The maximum K_p is displayed along with the propagation time, per event, in Figure 13. The events with the largest propagation time errors also had the largest maximum K_p errors. This was due to overestimations of the CME velocities for these particular events, which forecast the arrival times too early, and the maximum K_p indices too large.

7.2. Expected Value for Clock-Angle Term

Using the expected value for the clock-angle term, the ensemble forecasts no longer predicted a maximum K_p of 9 for all of the events (Figure 12). The forecasts for 9 of the 15 events had accuracy such that the actual maximum K_p was within the range of the ensemble. The forecasts for 4 of the 8 events with actual maximum K_p indices less than 9 had the actual maximum K_p within the range of the ensemble, which was slightly better than the 3 of 8 for the completely southward magnetic field forecasts. But, the forecasts using the expected value for the clock-angle term tended to underestimate the maximum K_p indices for the events with actual maximum K_p indices of 9.

For the 15 CMEs, the average of the ensemble ranges was calculated to be 1.5 with a standard deviation of 1.4. The range was zero for 4 of the events, compared to 11 events for the completely southward magnetic field forecasts. For the events with non-zero uncertainties, the average of the ensemble ranges was calculated to be 2.0, which was slightly less than the 2.8 calculated using the completely southward magnetic field forecasts.

The mean absolute forecast error for the 15 CMEs was calculated to be 1.8, which was slightly larger than the 1.7 calculated using the completely southward magnetic field forecasts. The mean absolute forecast error for the events with actual maximum K_p indices of 9 was 0.7, which was greater than the 0.0 for the completely southward magnetic field forecasts. The mean absolute forecast error for the events with actual maximum K_p indices less than 9 was 2.8, which was less than the 3.1 for the completely southward magnetic field forecasts. This indicated that the forecasts completed using the expected value for the clock-angle term were less accurate than the forecasts completed using a completely southward magnetic field for the events with actual maximum K_p indices of 9, but were more accurate for the events with actual maximum K_p indices less than 9.

The maximum K_p forecasts for 8 of the 15 events were lowered by using the expected value for the clock-angle term, compared to the completely southward magnetic field forecasts. The forecasts were underestimated for 6 of the events, and 4 of the events were overestimated (events 1, 7, 9 and 14). The forecasts which were overestimated corresponded to the slower events where the velocities were greatly overestimated.

8. Conclusions

Ensemble forecasts were produced for 15 halo-CMEs using the WSA-ENLIL version 2.7 with Coned Model version 1.3. The ensemble forecasts consisted of the propagation times to the L_1 Lagrangian point and the associated maximum K_p indices due to the impact of the CMEs on the Earth's magnetosphere. The 100 sets of cone parameters were derived from LASCO C3 imagery via the Coned Model, and were used as input to WSA-ENLIL to calculate the propagation times and maximum K_p indices. The ensemble forecasts were compared to the actual propagation times and maximum K_p indices to test the accuracy of the ensemble forecasting approach.

The propagation time ensemble forecasts estimated 5 of 15 events with accuracy such that the actual propagation time was within the ensemble average plus or minus the ensemble standard deviation. All 5 of the events had actual propagation times between 30 and 46 *hours*. 8 of 15 events were forecast with accuracy such that the actual propagation time was within the range of the ensemble.

The mean absolute forecast error, for the 15 CMEs, was calculated to be 9.1 *hours*. This was greater than the mean absolute forecast error of 6.9 *hours* calculated for the analytic Cone Model by *Taktakishvili et al.* [2011], but less than the mean absolute forecast error of 11.2 *hours* calculated for the automatic Cone Model (Coned Model) using

the median values of the cone parameter distributions as the cone parameters for a single ENLIL run by *Taktakishvili et al.* [2011].

Perhaps the most important result of this analysis was the dynamic quantification of the forecast uncertainty derived strictly from measurements (LASCO imagery) of the particular CME of interest. The average of the standard deviations of the propagation time ensembles was calculated to be 4.6 *hours*, and the average of the ranges was calculated to be 22.2 *hours*. While these values were not a measure of the forecast accuracy, they did provide a measure of the uncertainty in the forecasts based on the uncertainty in the measurements of the initial conditions, and would provide useful information to operational forecasts of CMEs.

The maximum K_p indices were calculated using the maximum K_p index formula created by *Newell et al.* [2007]. With no magnetic field information available inside of the CME "cloud" from ENLIL, two separate forecasts were created using two different assumptions regarding the magnetic field of the CME. First, the magnetic field was assumed to be completely southward to develop a worst case scenario. Then, to develop a less-conservative forecast, the expected value of the clock-angle term in the *Newell et al.* [2007] formula was used, assuming a randomly oriented magnetic field with a uniform distribution.

For the forecasts using the completely southward magnetic field, the ensemble forecast predicted maximum K_p indices of 9 for all events, which was an overestimation for many of the events. 10 of the 15 events were forecast with accuracy such that the actual maximum K_p index was within the range of the ensemble forecast. The mean absolute forecast error was calculated to be 1.7, and the average of the ensemble ranges was 0.74. Many of the forecasts had non-zero uncertainties due to the overestimation of impacts using the completely southward magnetic field assumption.

Using the expected value for the clock-angle term in the *Newell et al.* [2007] maximum K_p index formula lowered the forecasts such that 9 was not predicted for every event, and 9 of the 15 events were forecast with accuracy such that the actual maximum K_p index was within the range of the ensemble. The mean absolute forecast error was calculated to be 1.8, and the average of the ensemble ranges was 1.5. The forecasts created using the expected value for the clock-angle term were more accurate than the forecasts created assuming the magnetic field was completely southward for the events with actual maximum K_p indices less than 9, but were less accurate for the events with actual maximum K_p indices of 9.

The next step in ensemble forecasting of CMEs using the WSA-ENLIL with Coned Model will be to update the Coned Model to allow for the location of the CME eruption (associated solar flare location) as well as any propagation information derived from STEREO to be taken into account when calculating the cone parameters. This analysis showed that the Coned Model tends to push the propagation axes of CMEs towards the Sun-Earth line, which may not always correspond to reality. An improvement in the direction of propagation should also improve the accuracy of the velocity estimations due to the fact that the cone parameters calculated by the Coned Model are interdependent. The next version of ENLIL will allow for an internal magnetic field structure in the CME "cloud", which may help to improve the maximum K_p forecasts by improving the magnetic field magnitude estimates.

Acknowledgments. The folks at the Air Force Institute of Technology would like to sincerely thank the Community Coordinated Modeling Center at the NASA Goddard Space Flight

Center for providing the AFIT graduate students with an opportunity to work on CCMC projects. The collaboration between AFIT and CCMC allowed for a unique research experience working with the leaders in space weather research, and will have a large impact on the future of space weather research conducted by the United States Air Force.

References

- Afraimovich, E., V. Demyanov, and T. Kondakova (2003), Degradation of GPS performance in geomagnetically disturbed conditions, *GPS Solutions*, 7(2), 109–119.
- Arge, C., and V. Pizzo (2000), Improvement in the prediction of solar wind conditions using near-real time solar magnetic field updates, *Journal of geophysical research*, 105, 10.
- Boteler, D., R. Pirjola, and H. Nevanlinna (1998), The effects of geomagnetic disturbances on electrical systems at the Earth's surface, *Advances in Space Research*, 22(1), 17–27.
- DelSole, T. (2005), Predictability and information theory. part ii: Imperfect forecasts, *Journal of the atmospheric sciences*, 62(9), 3368–3381.
- Dryer, M. (1974), Interplanetary shock waves generated by solar flares, *Space Science Reviews*, 15(4), 403–468.
- Falkenberg, T., A. Taktakishvili, A. Pulkkinen, S. Vennerstrom, D. Odstrcil, D. Brain, G. Delory, and D. Mitchell (2011), Evaluating predictions of icme arrival at earth and mars, *Space Weather*, 9(9), S00E12.
- Gopalswamy, N., A. Lara, S. Yashiro, M. Kaiser, and R. Howard (2001), Predicting the 1-au arrival times of coronal mass ejections, *Journal of Geophysical Research. A. Space Physics*, 106, 29.
- Gosling, J. (1993), The solar flare myth, *Journal of geophysical research*, 98(A11), 18,937–18.
- Leith, C. (1974), Theoretical skill of monte carlo forecasts(stochastic atmospheric processes), *Monthly Weather Review*, 102, 409–418.
- Newell, P., T. Sotirelis, K. Liou, C. Meng, and F. Rich (2007), A nearly universal solar wind-magnetosphere coupling function inferred from 10 magnetospheric state variables, *J. Geophys. Res.*, 112, 1–16.
- Odstrcil, D., and V. Pizzo (1999), Three-dimensional propagation of coronal mass ejections (CMEs) in a structured solar wind flow 1. CME launched within the streamer belt, *Journal of geophysical research*, 104(A1), 483–492.
- Pulkkinen, A., T. Oates, and A. Taktakishvili (2010), Automatic determination of the conic coronal mass ejection model parameters, *Solar Physics*, 261(1), 115–126.
- Smith, Z., and M. Dryer (1990), Mhd study of temporal and spatial evolution of simulated interplanetary shocks in the ecliptic plane within 1 au, *Solar Physics*, 129(2), 387–405.
- Taktakishvili, A., M. Kuznetsova, P. MacNeice, M. Hesse, L. Rastatter, A. Pulkkinen, A. Chulaki, and D. Odstrcil (2009), Validation of the coronal mass ejection predictions at the earth orbit estimated by enlil heliosphere cone model, *Space Weather*, 7.
- Taktakishvili, A., P. MacNeice, and D. Odstrcil (2010), Model uncertainties in predictions of arrival of coronal mass ejections at earth orbit, *Space Weather*, 8(6), S06,007.
- Taktakishvili, A., A. Pulkkinen, P. MacNeice, M. Kuznetsova, M. Hesse, and D. Odstrcil (2011), Modeling of coronal mass ejections that caused particularly large geomagnetic storms using enlil heliosphere cone model, *Space Weather*, 9(6), S06,002.
- Tascione, T. F. (1994), *Introduction to the space environment*, Krieger Publishing Company Malabar, Florida.
- Tóth, G., and D. Odstrcil (1996), Comparison of some flux corrected transport and total variation diminishing numerical schemes for hydrodynamic and magnetohydrodynamic problems, *Journal of Computational Physics*, 128(1), 82–100.
- Xie, H., L. Ofman, and G. Lawrence (2004), Cone model for halo CMEs: Application to space weather forecasting, *Journal of geophysical research*, 109(A3), A03,109.
- Zhao, X., S. Plunkett, and W. Liu (2002), Determination of geometrical and kinematical properties of halo coronal mass ejections using the cone model, *J. Geophys. Res.*, 107(1223), 10–1029.

D. Emmons, A. Acebal Air Force Institute of Technology, Dayton, Ohio, USA (daniel.emmons.1@us.af.mil).

A. Pulkkinen, A. Taktakishvili, P. MacNeice NASA Goddard Space Flight Center, Greenbelt, Maryland, USA.